PLANT SCIENCES

Jasmonate biosynthesis arising from altered cell walls is prompted by turgor-driven mechanical compression

Stefan Mielke[1], Marlene Zimmer[1], Mukesh Kumar Meena[1], René Dreos[2], Hagen Stellmach[3], Bettina Hause[3], Cătălin Voiniciuc[4], Debora Gasperini[1]*

Despite the vital roles of jasmonoyl-isoleucine (JA-Ile) in governing plant growth and environmental acclimation, it remains unclear what intracellular processes lead to its induction. Here, we provide compelling genetic evidence that mechanical and osmotic regulation of turgor pressure represents a key elicitor of JA-Ile biosynthesis. After identifying cell wall mutant alleles in *KORRIGAN1* (*KOR1*) with elevated JA-Ile in seedling roots, we found that ectopic JA-Ile resulted from cell nonautonomous signals deriving from enlarged cortex cells compressing inner tissues and stimulating JA-Ile production. Restoring cortex cell size by cell type–specific KOR1 complementation, by isolating a genetic *kor1* suppressor, and by lowering turgor pressure with hyperosmotic treatments abolished JA-Ile signaling. Conversely, hypoosmotic treatment activated JA-Ile signaling in wild-type plants. Furthermore, constitutive JA-Ile levels guided mutant roots toward greater water availability. Collectively, these findings enhance our understanding on JA-Ile biosynthesis initiation and reveal a previously undescribed role of JA-Ile in orchestrating environmental resilience.

INTRODUCTION

In higher plants, the phytohormone (+)-7-*iso*-jasmonoyl-L-isoleucine (JA-Ile) is a decisive coordinator of growth and stress responses (*1*). Induced JA-Ile signaling secures a successful execution of reproductive development; regulates the acclimation to unfavorable conditions such as drought, salt, cold, elevated ozone, and ultraviolet light; and is essential to protect plants against insect herbivory, necrotrophic pathogens, and RNA viruses (*1*–*3*). It is estimated that insect herbivory alone affects >20% of global net plant productivity, and plants unable to synthesize JA-Ile, such as the *allene oxide synthase* (*aos*) mutant of the model plant *Arabidopsis thaliana*, are unprotected against chewing insects (*4*, *5*). Rising hormone levels elicit nuclear JA-Ile perception and signaling, leading to the increased expression of JA-Ile marker genes, such as *JASMONATE-ZIM DOMAIN 10* (*JAZ10*), and up-regulation of JA-Ile–induced defense transcripts such as *VEGETATIVE STORAGE PROTEIN 2* (*VSP2*) and *PLANT DEFENSIN 1.2* (*PDF1.2*) (*1*, *6*, *7*). As mounting defense responses are accompanied by reduced vegetative growth, JA-Ile levels are tightly regulated and normally induced only when required (*1*, *8*). Despite the broad and critical functions of the jasmonate (JA) pathway in plant growth and environmental acclimation, the intracellular events triggering JA-Ile production remain poorly understood (*1*, *9*, *10*).

Several molecular elicitors of JA-Ile biosynthesis have been proposed, including herbivore-, microbe-, and damage-associated molecular patterns generated during environmental stresses. These elicitors would be recognized by putative pattern recognition receptors at the cell surface that transduce the signal intracellularly and initiate de novo JA-Ile synthesis, reviewed in (*9*, *11*). However, conclusive genetic evidence for ligand-based induction of JA-Ile biosynthesis is still missing. Mechanical wounding is another potent activator of JA-Ile biosynthesis and is widely used to stimulate endogenous hormone production (*6*, *10*). In parallel to necrotroph and herbivorous insect attacks, mechanical wounding causes the disruption of cell walls that surround each plant cell and serve as the immediate contact surface with the extracellular environment. Plant cell walls are elaborate structural networks consisting predominantly of complex polysaccharides (cellulose, hemicelluloses, and pectins), a lower amount of proteins, and other soluble and phenolic materials (*12*). Notably, chemical or genetic inhibition of cellulose biosynthesis by isoxaben application or by mutations in *CELLULOSE SYNTHASE* (*CesA*) genes leads to increased JA-Ile levels, e.g., (*11*, *13*, *14*). Consistently, mutations in *KORRIGAN1* (*KOR1*), a CesA-interacting membrane protein with endo-1,4-β-D-glucanase activity involved in cellulose biosynthesis, exhibit a slight basal increase in the JA-Ile precursor JA (*15*–*19*). Nevertheless, it remains unclear how cellulose deficiency stimulates JA-Ile production and in which plant tissues the hormone accumulates.

Plant cells have a high intracellular turgor pressure deriving from a gradient in osmotic potential across the plasma membrane, which is counterbalanced by their cell walls, with cellulose microfibrils serving as a load-bearing component (*12*). If osmotic conditions change, then plant cells may experience mechanical stress and even deform their shape depending on the extent of the stimulus, their geometry, and the properties of their cell walls. Hence, they regulate water and ionic fluxes across the plasma membrane and remodel their cell wall until a new osmotic equilibrium is reached and turgor pressure is reestablished (*20*, *21*). Cell walls with compromised cellulose microfibrils may be inefficient at counteracting the high intracellular turgor pressure, resulting in enlarged cells. Cell swelling is, in fact, a typical feature observed in cellulose-deficient mutants or isoxaben-treated plants (*22*, *23*). Mechanical stress arising from turgor pressure changes might be therefore involved in activating JA-mediated stress responses (*24*). In fact, cotreatments of liquid-grown seedlings with isoxaben and sorbitol serving as osmotica nullify the increased JA levels induced by isoxaben alone (*23*, *25*), linking osmoregulation to the JA pathway.

[1]Department of Molecular Signal Processing, Leibniz Institute of Plant Biochemistry, 06120 Halle (Saale), Germany. [2]Center for Integrative Genomics, University of Lausanne, 1015 Lausanne, Switzerland. [3]Department of Cell and Metabolic Biology, Leibniz Institute of Plant Biochemistry, 06120 Halle (Saale), Germany. [4]Independent Junior Research Group–Designer Glycans, Leibniz Institute of Plant Biochemistry, 06120 Halle (Saale), Germany.
*Corresponding author. Email: debora.gasperini@ipb-halle.de

Here, we investigated how cues derived from perturbed cellulose biosynthesis integrate with JA-Ile production. First, we identified *kor1* alleles with increased JA-Ile levels in cell type–specific contexts of the primary root. While elevated JA-Ile signaling in *kor1-4* was confined to inner root tissues, restoring KOR1 function in adjacent cortex cells complemented the JA phenotype. Transversal sections revealed a pronounced enlargement of cortex cells, likely exerting mechanical pressure on physically constrained inner tissues. Reducing cortex cell size by genetic and chemical means fully abolished expanded *kor1* cortex cells and constitutive JA-Ile signaling, indicating that JA biosynthesis is triggered by turgor-driven mechanical compression. Consistently, increasing turgor pressure with hypoosmotic treatment activated JA-Ile signaling in inner root tissues of wild-type (WT) plants. While constitutive JA-Ile signaling did not affect *kor1* root growth rate nor the expression of JA-dependent defense genes, it was critical to guide root growth toward greater water availability.

RESULTS

Cellulose-deficient *kor1* mutants have increased root JA-Ile levels

In a forward genetic screen aimed at identifying negative regulators of JA signaling (*6*), we isolated two alleles of *KOR1*, *kor1-4* and *kor1-5*, exhibiting ectopic expression of the JA-responsive reporter *JAZ10p:GUSPlus* (*JAZ10p:GUS*, *JGP*). Basal *JGP* expression in the WT and in JA-deficient *aos* plants is very weak, whereas *kor1* alleles showed *JGP* activation in the primary root (Fig. 1A and fig. S1A). Allelism tests with a transfer DNA (T-DNA) insertion *kor1-6* mutant in the *JGP* background and complementation by transformation with untagged (*KOR1p:KOR1*) and N-terminal CITRINE (CIT)–tagged KOR1 (*KOR1p:CIT-KOR1*) constructs, both restoring the *kor1* short root length, confirmed the causative mutations of the observed *JGP* phenotype (Fig. 1, A and B). Ethyl methanesulfonate (EMS) *kor1* alleles harbored single amino acid exchanges within the extracellular GLYCOSYL HYDROLASE 9 (GH9) domain of KOR1 (L573F in *kor1-4* and P172L in *kor1-5*), while *kor1-6* resulted in lower *KOR1* transcript levels (fig. S1, B and C). Among the three *kor1* alleles, *kor1-5* showed the most severe JA and root elongation phenotypes and *kor1-6* the mildest (Fig. 1, A and C, and fig. S1, A and D), implying that all mutants still retain partial KOR1 function. This is in line with previous reports proposing that full *KOR1* knockouts are lethal (*16*). Given the milder growth defects and robust JA phenotype of *kor1-4*, we used this allele for further analyses.

Despite the broad *KOR1* expression domain and stunted shoot growth phenotypes of characterized mutants (*26*), constitutive *JGP* activation was not detected in aerial tissues of *kor1* alleles (Fig. 1A and fig. S1A). Shoot wounding and exogenous MeJA treatment promptly induced *JGP* reporter expression across *kor1* tissues, validating the root specificity of basal *JGP* activity (Fig. 1A and fig. S1A). Quantitative analysis of *JAZ10* transcripts further supported the specific activation of JA signaling in roots but not shoots of all three *kor1* alleles (Fig. 1C). This phenotype was dependent on JA-Ile production, as increased reporter activity and *JAZ10* transcript levels were abolished in JA-deficient *kor1 aos* double mutants (Fig. 1A and fig. S1, A, E, and F). In addition to *JAZ10*, *kor1-4* exhibited increased root expression of JA marker transcripts *JASMONATE OXYGENASE 3* (*JOX3*) and *JAZ3* in a JA-dependent manner, as well as increased levels of the bioactive JA-Ile conjugate (Fig. 1, D and E, and fig. S1G). Collectively, our data indicate that KOR1 is a negative regulator of root JA-Ile biosynthesis. Hence, *kor1* mutants represent valuable genetic tools to study how cell wall–derived signals are integrated with intracellular hormone production and uncover JA-Ile functions in moderating root responses to cellulose deficiency.

Cortex-specific KOR1 expression complements ectopic JA signaling in *kor1* endodermis and pericycle

To map the precise tissues and cell types displaying ectopic JA signaling in *kor1-4* roots, we used a transcriptional reporter expressing three VENUS (3xVEN) fluorescent proteins fused N-terminally to a NUCLEAR LOCALIZATION SIGNAL (NLS) under the control of *JAZ10p* (*JAZ10p:NLS-3xVEN*) (*27*). Similar to *JGP*, *JAZ10p:NLS-3xVEN* expression was not detectable at basal conditions but increased notably after MeJA treatment in both WT and *aos* roots, while mechanical wounding triggered *JAZ10p:NLS-3xVEN* induction in the WT but not in *aos* (Fig. 2A and fig. S2). In contrast to the WT, *kor1-4* exhibited constitutive *JAZ10p:NLS-3xVEN* expression predominantly in the early differentiation zone of the primary root, mostly confined to endodermal and pericycle cells (Fig. 2, A to C). The extent of activated JA signaling was quantified by evaluating the presence of *JAZ10p:NLS-3xVEN* along longitudinal cell files and displaying the resulting frequency in a heatmap for each cell layer (Fig. 2D). Weak reporter activation coincided with the onset of cell elongation and proceeded longitudinally into the early differentiation zone for approximately 30 cells before ceasing. While only <10% of *kor1-4* roots showed sporadic *JAZ10p:NLS-3xVEN* expression in a few epidermal or cortex cells, the majority of individuals displayed consistent JA signaling in a stretch of 10 to 15 endodermal and pericycle cells in the root early differentiation zone (Fig. 2D).

Because JA-Ile precursors can relocate across tissues (*28*, *29*), increased JA signaling in different cell types could result from cell-autonomous or non–cell-autonomous signals. To discriminate between these two possibilities and identify the source tissue responsible for increased JA-Ile biosynthesis, we drove the expression of a functional CIT-KOR1 fusion protein under the control of cell type–specific promoters and evaluated its capacity to complement ectopic *JGP* expression in *kor1-4*. As expected, when driven by its endogenous promoter (*KOR1p*), CIT-KOR1 expression was detectable across the entire root, and respective cell type–specific promoters resulted in CIT-KOR1 expression at the intended locations: *IRON-REGULATED TRANSPORTER 1* (*IRT1p*) in the epidermis, *PLASTID ENDOPEPTIDASE* (*PEPp*) in the cortex, *SCARECROW* (*SCRp*) in the endodermis, and *WOODEN LEG 1* (*WOL1p*) or *PIN-FORMED 1* (*PIN1p*) in the stele, which includes the pericycle (fig. S3, A to E) (*26*, *30*). Intriguingly, ectopic *JGP* expression in *kor1-4* was complemented only when expressing CIT-KOR1 in the cortex (*PEPp:CIT-KOR1*), but not in the epidermis (*IRT1p:CIT-KOR1*), nor in endodermal (*SCRp:CIT-KOR1*) or pericycle (*WOLp:CIT-KOR1* or *PIN1p:CIT-KOR1*) cells that exhibited high JA signaling (Fig. 2E). Furthermore, the short root *kor1-4* phenotype was ameliorated by expressing CIT-KOR1 in the cortex, while it remained unchanged when expressing the construct in the epidermis, and it was even slightly exacerbated by cell type–specific expression in the endodermis or pericycle (fig. S3F). These results suggest that maintaining KOR1 functionality in the cortex is critical for impeding the activation of JA-Ile production in adjacent endodermal and pericycle cells.

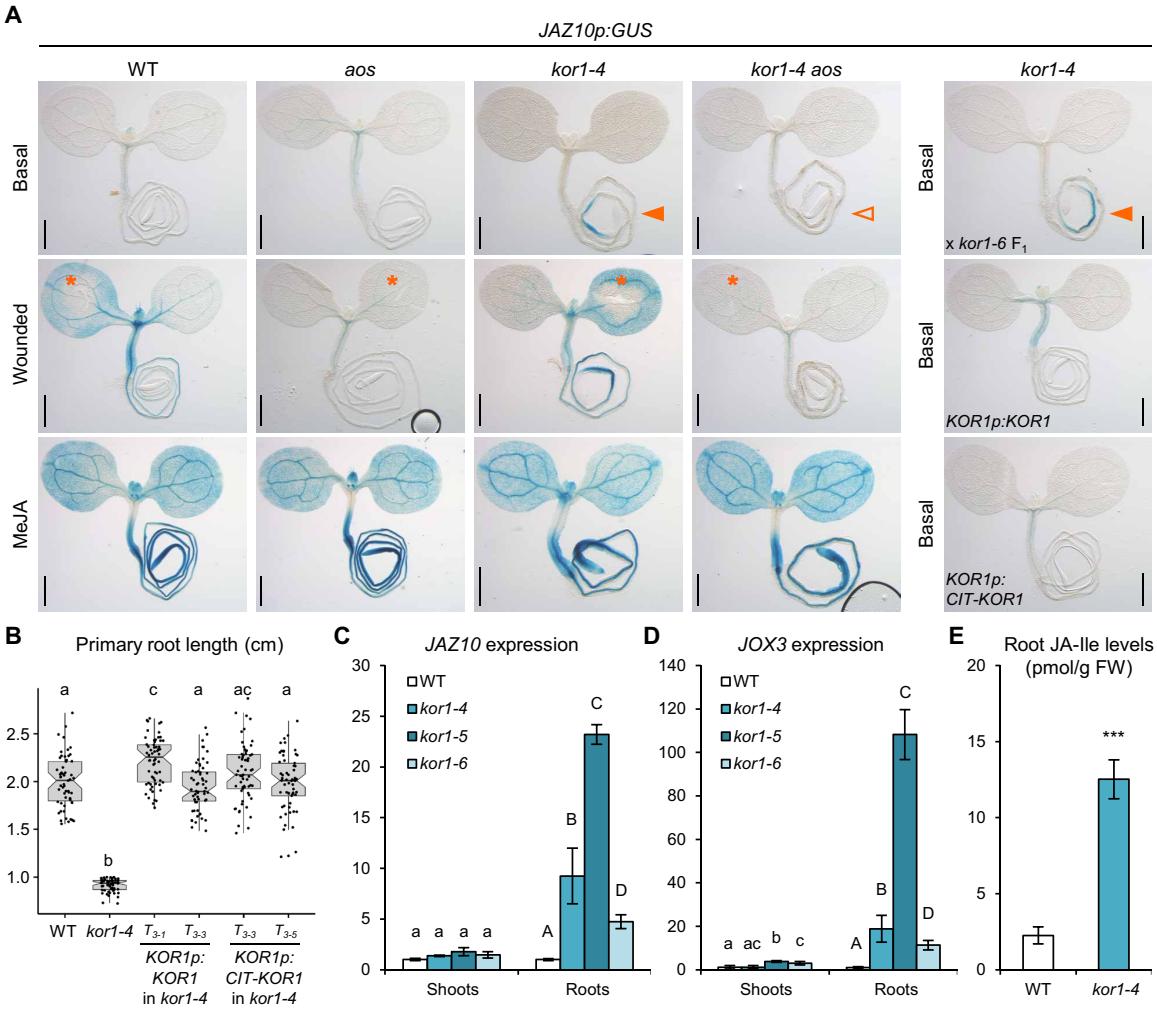

Fig. 1. *kor1* mutant roots display increased JA-Ile levels and signaling. (**A**) Representative *JAZ10p:GUS (JGP)* reporter activity in 5-do seedlings of WT, *aos*, *kor1-4*, *kor1-4 aos* at basal conditions, 2 hours after cotyledon wounding (orange asterisks), 2 hours after 25 μM MeJA treatment, and in *kor1-4* x *kor1-6* F_1 (allelism test), *kor1-4* complemented with *KOR1p:KOR1* and *KOR1p:CIT-KOR1* lines. Note the increased *JAZ10p:GUS* reporter activity in *kor1-4* and allelism test (orange arrowheads) and its absence from *kor1-4 aos* (empty arrowhead). Scale bars, 0.5 mm. (**B**) Primary root length box plot summary in 7-do WT, *kor1-4*, and two independent T_3 lines for each complementing *KOR1p:KOR1* and *KOR1p:CIT-KOR1* construct. Both constructs restored the *kor1-4* short root phenotype to WT length. Medians are represented inside the boxes by solid lines, and circles depict individual measurements ($n = 59$ to 61). (**C** and **D**) Quantitative reverse transcription polymerase chain reaction (qRT-PCR) of basal (C) *JAZ10* and (D) *JOX3* expression in shoots and roots of WT and three *kor1* mutant alleles. *JAZ10* and *JOX3* transcript levels were normalized to those of *UBC21*. Bars represent the means of three biological replicates (±SD), each containing a pool of ~60 organs from 5-do seedlings. (**E**) Absolute JA-Ile content in WT and *kor1-4* roots. Bars represent the means of three biological replicates (±SD), each containing a pool of ~600 roots from 5-do seedlings. Letters and asterisks denote statistically significant differences among samples as determined by analysis of variance (ANOVA) followed by Tukey's honest significant difference (HSD) test ($P < 0.05$) in (B) to (D) and by Student's *t* test ($P = 0.0005$) in (E).

Mutations in *ESMD1* suppress elevated JA signaling levels in *kor1*

To identify genetic regulators of JA-Ile production in *kor1*, we performed an EMS suppressor screen in *kor1-4 JGP* for lack of JA reporter activation. Mapping by whole-genome-sequencing of bulk segregants isolated an allele in *ESMERALDA1* (*ESMD1*), which we named *esmd1-3*. The *esmd1-3* allele abolished the constitutive *JGP* expression and high *JAZ10* levels in *kor1-4* roots while retaining the capacity to induce *JAZ10* transcripts after wounding (Fig. 3, A and B, and fig. S4, A to C). An ESMD1-mTURQUOISE2 (mT) fusion protein expressed under the *ESMD1p* native promoter restored the ectopic JA signaling in *kor1-4 esmd1-3* (Fig. 3A and fig. S4A). Consistently, introgressing another *esmd1-1* EMS allele (*31*) into *kor1-4* partially suppressed the elevated *JAZ10* levels in *kor1-4* (Fig. 3B), confirming the suppressor's identity and causative amino acid R373C substitution in *esmd1-3* (fig. S4D). As we could not retrieve homozygous mutants from a segregating T-DNA population in *ESMD1* (*esmd1-4*) (fig. S4D), and *esmd1-1* was a weaker JA suppressor than *esmd1-3*, it is likely that full loss of ESMD1 function leads to lethality and that both EMS alleles used here are partial loss of function. *ESMD1* is a member of the plant-specific glycosyltransferase GT106 family, with putative *O*-fucosyltransferase activity involved in regulating pectin homeostasis (*31*, *32*). Specifically, *esmd1* was identified as a suppressor of the stunted growth phenotypes of mutants deficient in the major pectin constituent homogalacturonan (HG) (*31*). Because *esmd1* restored the cell-to-cell adhesion defects

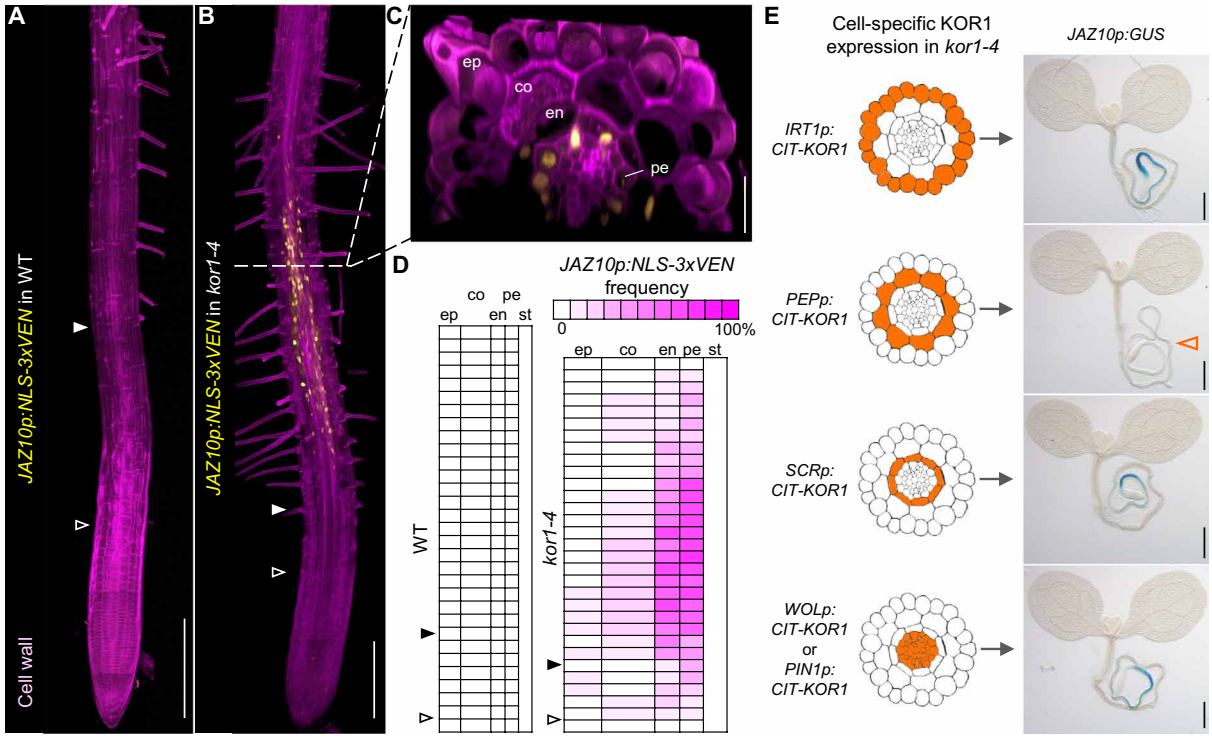

Fig. 2. Cortex-specific expression of CIT-KOR1 complements increased JA signaling in endodermis and pericycle of *kor1-4*. (**A** to **C**) *JAZ10p:NLS-3xVEN* expression in 5-do (A) WT and (B and C) *kor1-4* roots cleared with ClearSee, counterstained with the cellulose dye Direct Red 23, and visualized as three-dimensional Z-stacks. (C) Orthogonal view from the epidermis to the vascular cylinder of *kor1-4*. The onset of elongation is indicated by empty arrowheads (first elongated cortex cell), and that of differentiation by filled arrowheads (appearance of root hairs). ep, epidermis; co, cortex; en, endodermis; pe, pericycle. (**D**) Heatmap of *JAZ10p:NLS-3xVEN* frequency in individual cells from WT and *kor1-4* primary roots ($n = 21$). Presence or absence of the reporter was evaluated from the onset of elongation in individual cells along consecutive longitudinal files for each tissue layer. Reporter expression was not observed in the WT nor in *kor1-4* vascular tissues of the stele (st). (**E**) Cell-specific complementation of *JAZ10p:GUS (JGP)* activity in *kor1-4* by expressing CIT-KOR1 in either epidermis (*IRT1p:CIT-KOR1*), cortex (*PEPp:CIT-KOR1*), endodermis (*SCRp:CIT-KOR1*), or stele (*WOLp:CIT-KOR1* or *PIN1p:CIT-KOR1*). Note that cortex-expressed CIT-KOR1 complements *JAZ10p:GUS* activity in *kor1-4,* as indicated by lack of the *JAZ10p:GUS* reporter in representative images from T_3 lines (empty orange arrowhead). A minimum of 30 T_3 individuals were analyzed for each line. Scale bars, 200 μm (A and B), 30 μm (C), and 0.5 mm (E).

without complementing the low HG content of pectin mutants *quasimodo1* (*qua1,* a putative galacturonosyltransferase of the glycosyltransferase GT8 family) and *quasimodo2* (*qua2,* a methyltransferase) (*31*, *33*–*35*), we wondered whether, in addition to suppressing JA signaling, *esmd1-3* was able to revert other *kor1-4* phenotypes.

Contrary to ameliorating *qua1* and *qua2* growth phenotypes (*31*), *esmd1-3* did not restore the short root length nor the cellulose deficiency in shoots and roots of *kor1-4* seedlings (Fig. 3, C and D, and fig. S4E). On the basis of previous reports (*31*), we expected similar neutral and acidic sugar profiles from cell walls of genotypes with *esmd1-3*. Instead, monosaccharide analysis of cell walls from shoots and roots revealed some significant changes in matrix polysaccharide composition between WT and certain mutants (Fig. 3E and fig. S4F). Most notably, the *esmd1-3* mutation reduced rhamnose abundance (by 32 to 38% in roots and 15% in shoots) with respect to the WT (Fig. 3E and fig. S4F). Because cellulose deficiency often leads to ectopic lignification (*36*), we next evaluated lignin deposition in our mutant set. Phloroglucinol staining revealed patches of lignified cells across the primary root of *kor1-4* that were absent in WT and *aos* plants (Fig. 3F and fig. S4G). The ectopic lignification in *kor1-4* was not a consequence of elevated JA levels as *kor1-4 aos* still exhibited lignified cells, and was entirely abolished in *kor1-4 esmd1-3*. Overall, the cell wall analysis indicated an elaborate compensatory network in *kor1 esmd1*. The *kor1* mutation was epistatic to *esmd1* in terms of short root length and cellulose deficiency, while *esmd1* was epistatic to *kor1* with respect to lack of increased JA signaling, reduced rhamnose abundance, and lack of ectopic lignification. The results therefore suggest that increased JA signaling in *kor1* may be due to indirect consequences of cellulose deficiency on cell wall architecture and mechanical properties, rather than to altered levels of a specific cell wall component.

To gain further insights into how ESMD1 may influence JA responses in *kor1*, we concentrated on its localization in the primary root. Although an ESMD1–green fluorescent protein fusion protein was expressed in the Golgi when transiently overexpressed in leaf epidermal cells of *Nicotiana benthamiana* (*31*), we were unable to visualize the functional *ESMD1p:ESMD1-mT* construct nor *ESMDp:ESMD1-CIT* in WT *Arabidopsis* roots, suggesting that ESMD1 levels are very low and/or tightly regulated. Instead, *ESMD1p:NLS-3xVEN* expression was mapped to older parts of the root as expected (*31*) and to the epidermis, cortex, and endodermis of the early differentiation zone (Fig. 3, G to I).

Enlarged *kor1* cortex cells affect JA production in inner tissues

Having found that *ESMD1* expression includes our zone of interest, we further noticed that *kor1-4 esmd1-3* roots are considerably thinner

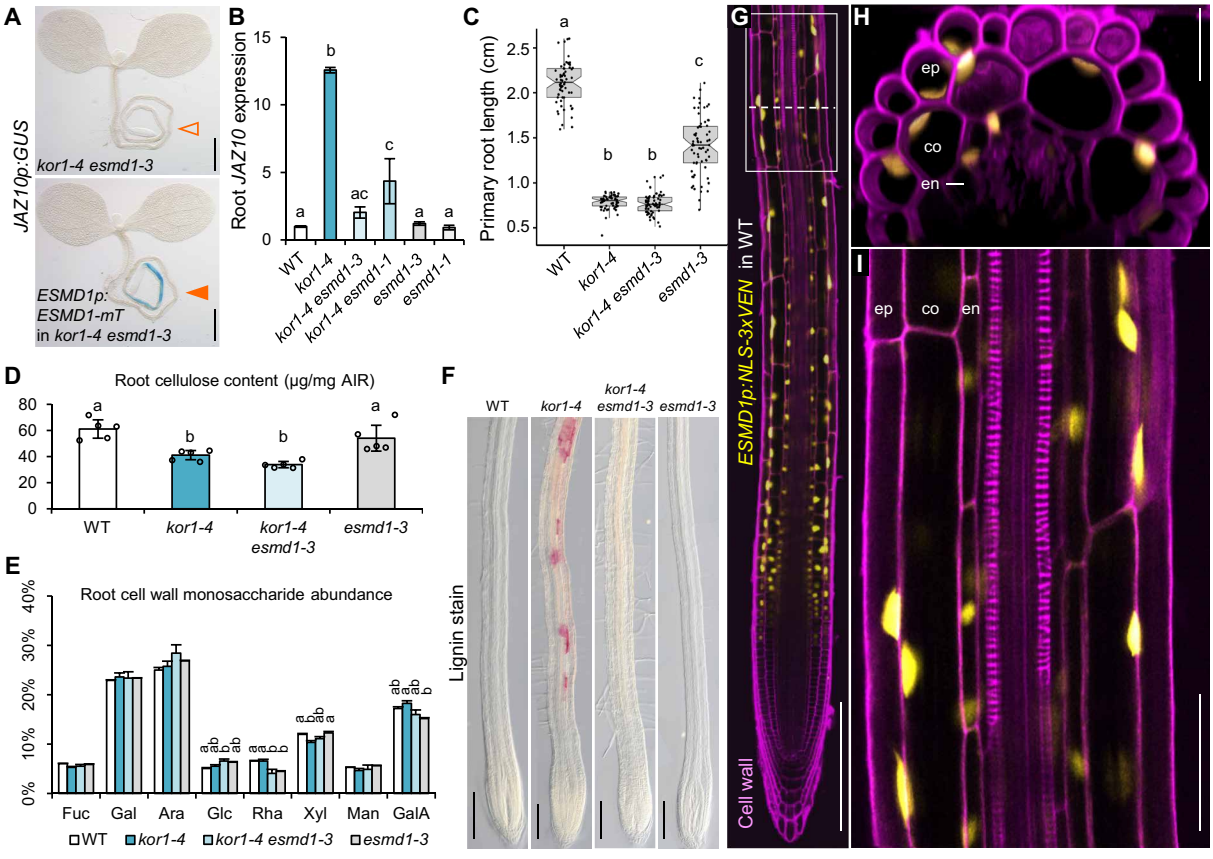

Fig. 3. *ESMD1* is a positive regulator of ectopic JA-Ile production in *kor1*. (**A**) *JAZ10p:GUS* expression is absent in *kor1-4 esmd1-3* (empty arrowhead) and present in its *ESMD1p:ESMD1-mTurquoise* (*mT*) complementation line (orange arrowhead). (**B**) qRT-PCR of basal *JAZ10* expression in roots of indicated genotypes. *JAZ10* transcript levels were normalized to *UBC21*. Bars represent the means of three biological replicates (±SD), each containing ~60 roots from 5-do seedlings. (**C**) Primary root length box plots from 7-do seedlings of indicated genotypes. Medians are represented inside the boxes by solid lines, and circles depict individual measurements ($n = 58$ to 66). (**D**) Crystalline cellulose content from alcohol-insoluble residue (AIR) extracted from roots of indicated genotypes. Bars represent means of five biological replicates depicted as circles (±SD), each consisting of pools from ~300 roots from 12-do seedlings. (**E**) Cell wall monosaccharide composition analysis from root-extracted AIR of indicated genotypes. Bars represent the means of three biological replicates (±SD). Only statistically significant differences among genotypes indicated with letters and assessed for each individual sugar are shown above bars. Fuc, fucose; Gal, galactose; Ara, arabinose; Glc, glucose; Rha, rhamnose; Xyl, xylose; Man, mannose; GalA, galacturonic acid. (**F**) Lignin deposition visualized by phloroglucinol stain (fuchsia) in primary roots of indicated genotypes. (**G** to **I**) *ESMD1p:NLS-3xVEN* expression in 5-do WT primary roots counterstained with PI. (H) Orthogonal view from epidermis to vascular cylinder of a Z-stack section in the early differentiation zone through (G) (dotted line). (I) Increased magnification from (G) (boxed). ep, epidermis; co, cortex; en, endodermis. Letters in (B) to (E) denote statistically significant differences among samples as determined by ANOVA followed by Tukey's HSD test [$P < 0.05$ and $P < 0.001$ in (E)]. Scale bars, 0.5 mm (A), 200 µm (F and G), 25 µm (H), and 50 µm (I).

than *kor1-4* (Fig. 4, A and B). Transversal sections across the root early differentiation zone coinciding with the sites of JA production in *kor1-4* revealed that root thickness in the mutant was twice that of the WT and resulted from enlarged areas of all cell types examined (Fig. 4, C and D, and fig. S5, A to F). The relatively small expansion of *kor1-4* epidermal cell area (1.1-fold) was counterbalanced by a significant increase in their cell number (fig. S5, A and C). Although aberrant cell divisions were also occasionally observed in *kor1-4* cortex and endodermal cells, the overall cell number in these cell types did not differ significantly from the WT (fig. S5A). The largest augmentation in *kor1-4* cell area was found for cortex cells, being 2.6-fold larger than WT, while endodermal and pericycle cells displayed an expansion of 2- and 2.4-fold, respectively (Fig. 4, C and D, and fig. S5, C to F). These *kor1-4* phenotypes were almost completely restored to WT levels in the *kor1-4 esmd1-3* suppressor, which showed a diminished root thickness; a full complementation of epidermal cell numbers; and reduced cell areas of cortex, endodermis, and pericycle cells (Fig. 4, A to D, and fig. S5, A to F). Notably, the large expansion of *kor1-4* cortex cells was drastically reduced in *kor1-4 esmd1-3* (Fig. 4, C and D), leading us to hypothesize that enlarged cortex cells may impinge upon inner tissues.

To verify whether *kor1-4* enlarged cortex cells indeed affected JA-Ile production in inner epidermal and pericycle tissues, we analyzed our transgenic lines expressing CIT-KOR1 under cell type–specific promoters in transversal root sections coinciding with ectopic JA production (Fig. 2). As expected, expressing CIT-KOR1 under its native promoter fully restored *kor1-4* root thickness to WT dimensions, while epidermis-, cortex-, and endodermis-specific CIT-KOR1 expression reduced *kor1-4* root thickness to various degrees. Stele-specific CIT-KOR1 expression (st-*WOLp*) did not have any significant effect and was thus excluded from further analysis (Fig. 4, A and B). Compared to the *KOR1p:CIT-KOR1* complemented *kor1-4* line, epidermal CIT-KOR1 expression (ep-*IRT1p*) still exhibited typical *kor1-4* features of twofold enlarged root area; increased epidermal

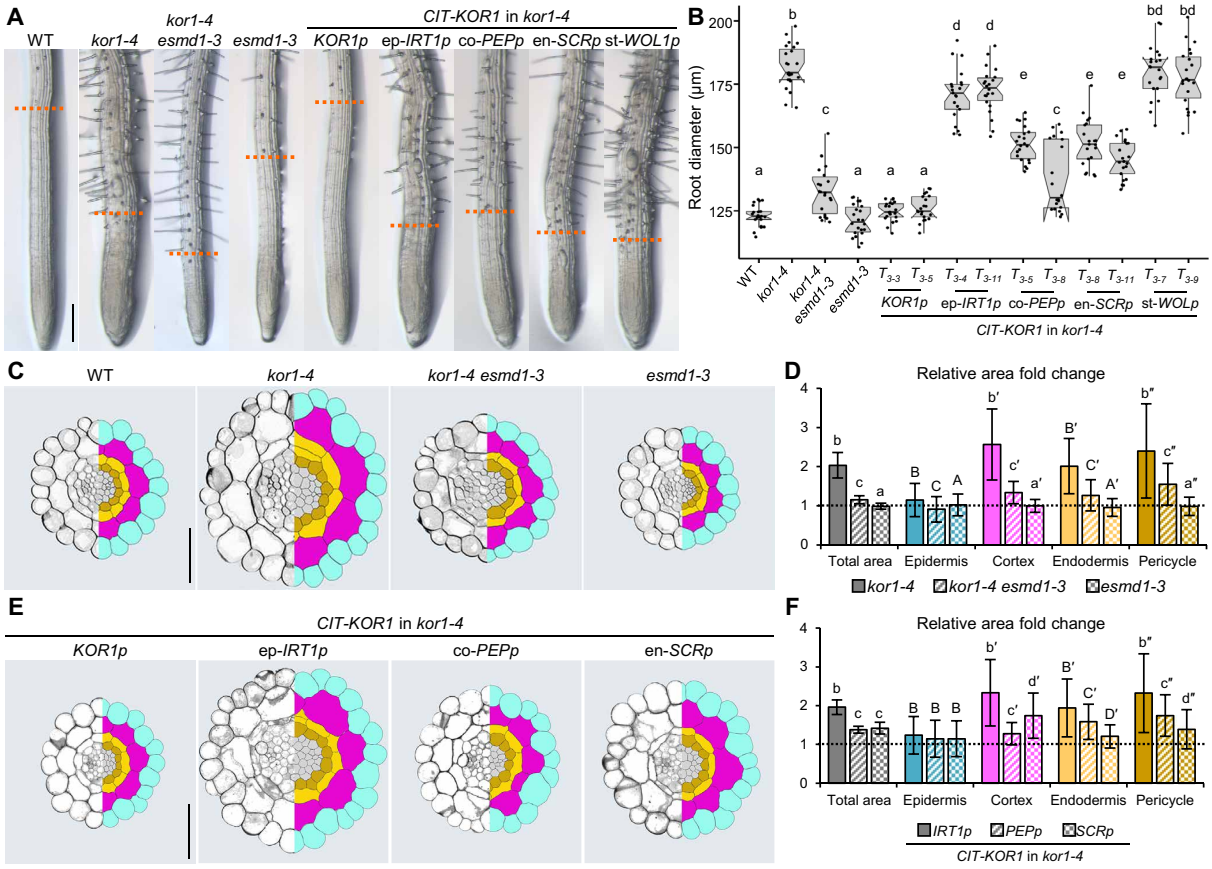

Fig. 4. Cortex cell enlargement in *kor1* correlates with constitutive JA production. (**A**) Representative primary root images of WT, *kor1-4*, *kor1-4 esmd1-3*, *esmd1-3*, and *kor1-4* complemented with CIT-KOR1 under the control of its native *KOR1p* promoter, or epidermis (ep-*IRT1p*)–, cortex (co-*PEPp*)–, endodermis (en-*SCRp*)–, or stele (st-*WOL1p*)–specific promoters. Orange dashed lines define the initiation of the differentiation zone, as indicated by the appearance of root hairs in 7-do seedlings. (**B**) Box plot summary of primary root diameter at the onset of differentiation in 7-do seedlings of indicated genotypes. Medians are represented inside the boxes by solid lines, and circles depict individual measurements ($n = 22$ to 23). (**C** to **F**) Anatomy and cell size comparisons from transverse sections across the early differentiation zone of the primary root in (C and D) WT, *kor1-4*, *kor1-4 esmd1-3*, and *esmd1-3*, and in (E and F) *kor1-4* complemented with cell type–specific promoters. (C and E) Representative split images from cross sections (left) and respective cell segmentations (right). Segmented cell types are color-coded as: epidermis, turquoise; cortex, magenta; endodermis, yellow; pericycle, mustard; stele, gray. (D and F) Fold change in total and cell-specific areas from segmented transversal root sections in indicated genotypes. Bars represent mean fold changes of individual cellular areas from 10 to 11 roots (±SD), normalized to values of the (D) WT or (F) *KOR1p:CIT-KOR1* indicated by dashed lines (individual measurements are available in fig. S5). Letters in (B), (D), and (F) denote statistically significant differences among samples as determined by ANOVA followed by Tukey's HSD test ($P < 0.05$). Scale bars, 200 µm (A) and 50 µm (C and E).

cell number; and enlarged areas of cortex, endodermal, and pericycle cells (Fig. 4, E and F, and fig. S5, G to L). Conversely, expressing CIT-KOR1 in either cortex (co-*PEPp*) or endodermal (en-*SCRp*) cell layers rendered *kor1-4* phenotypes more similar to the *KOR1p:CIT-KOR1* complemented *kor1-4* line by showing a 1.4-fold increase in total root area and only a milder enlargement of cortex, endodermis, and pericycle cells (Fig. 4, E and F, and fig. S5, G to L). While the most prominent effect of expressing CIT-KOR1 in cortex or endodermis was to reduce the area of cells in which the fusion protein was localized, the strongest correlation between JA signaling and cell type area was again found for the cortex cell layer. Expressing CIT-KOR1 in the cortex (co-*PEPp*) abolished *kor1-4 JGP* expression and restored cortex cell area to almost WT levels (1.2-fold) without fully recovering cellular enlargement of endodermal and pericycle cells, which persisted being 1.6- and 1.7-fold larger than the *KOR1p:CIT-KOR1* complemented line (Figs. 2E and 4, E and F). In turn, endodermal CIT-KOR1 expression (en-*SCRp*) did not abolish elevated JA levels in *kor1-4* nor led to a drastic reduction in cortex expansion that remained 1.7-fold larger, albeit almost completely restoring endodermal and pericycle cell areas (Figs. 2E and 4, E and F). As KOR1 activity in cortex cells is important to regulate their size and *JGP* expression in adjacent inner tissues, and *ESMD1* is expressed in both cortex and endodermal cells, it is conceivable that the cortex-endodermis interface is critical for governing JA-Ile production in *kor1*.

Osmotically driven turgor pressure changes regulate JA-Ile signaling in *kor1* and WT

JA responses can be triggered by exogenous treatment with specific pectin- and cellulose-derived fragments serving as ligands binding putative plasma membrane receptors and activating intracellular signaling, reviewed in (*11*). More notoriously, JA-Ile biosynthesis is swiftly activated by mechanical stress (*24*). The morphological changes in cellular areas across root transversal sections (Fig. 4) led us to hypothesize that increased JA-Ile levels in *kor1* may result from enlarged cortex cells "squeezing" spatially constrained inner

tissues, rather than from cell wall–derived elicitors. To test this hypothesis, we decreased intracellular turgor pressure by growing *kor1-4* seedlings under hyperosmotic conditions to withdraw water from their cells. All tested substances acting as osmotica [mannitol, sorbitol, polyethylene glycol (PEG), hard agar] effectively abolished JA signaling in *kor1-4* roots (Fig. 5, A and B, and fig. S6A). Mannitol-grown seedlings still responded to wounding, reinforcing the tissue specificity of the *JGP* reporter (fig. S6B). Furthermore, while WT root length decreased under hyperosmotic conditions, *kor1-4* root elongation exhibited a tangible amelioration (Fig. 5C). This was also reflected in the reduced area of *kor1-4* transversal root sections grown on mannitol reverting to WT size (Fig. 5, D and E). Consistently, mannitol treatment restored *kor1-4* epidermal cell number as well as enlarged epidermal, cortex, endodermis, and pericycle cell size (Fig. 5, D and E, and fig. S6, C to H). Notably, the hyperosmotic treatment fully recovered the enlarged *kor1-4* cortex cell area to WT levels, while endodermal and pericycle cells were still 1.2-fold larger with respect to the WT (Fig. 5, D and E). Thus, the activation of JA production in *kor1* is consistent with inner tissues being mechanically stressed by enlarged cortex cells.

We then reasoned that changes in turgor pressure leading to cellular enlargement, such as those driven by hypoosmotic treatments that stimulate cellular water uptake, may cause mechanical stress within tissues and result in JA-Ile biosynthesis even in WT plants. Transferring WT *JGP* reporter seedlings to deionized water indeed resulted in reporter activation, which increased over time and encompassed the root and portions of the shoot apical meristem (Fig. 5F). Because the *JGP* reporter is suited to reveal JA-Ile signaling in tissues but not to map cellular expression sites (*6*), we verified which cells activated JA-Ile signaling with the *JAZ10p:NLS-3xVEN* reporter. While a 24-hour treatment in isotonic mock solution did not affect *JAZ10p:NLS-3xVEN* expression, hypoosmotic treatment severely damaged the root apical meristem (RAM) as indicated by propidium iodide (PI) penetration and activated the reporter in internal root tissues (Fig. 5, G and H). Notably, although *JAZ10p:NLS-3xVEN* expression can be induced in every cell type of the primary root (fig. S2), the hypoosmotic treatment triggered JA-Ile signaling predominantly in endodermal and pericycle cells starting at the root early differentiation zone (Fig. 5, H to J). Overall, our data indicate that osmotically driven turgor pressure changes have a remarkable impact on JA-Ile production.

Heightened JA levels guide *kor1* roots toward greater water availability

The activation of JA signaling often leads to an induction in defense responses accompanied by a reduction in organ growth (*37*). *kor1-4* root meristem length was significantly shorter than the WT, while its cell number remained unchanged (fig. S7, A to C). It is thus possible that increased JA production in *kor1* contributes to slow down the mutant's root growth rate to better adjust to cellulose deficiency and concomitantly protect the mutant from potential threats found in the soil. However, blocking JA production in *kor1-4* did not alter root elongation nor the expression of JA-dependent defense marker genes, as the mutant had the same root growth rate as its JA-deficient *kor1-4 aos* counterpart and similar low basal levels of *VSP2* and *PDF1.2* transcripts (Fig. 6A and fig. S7, D and E).

As the stunted *kor1-4* root growth was alleviated by continuous growth in mannitol (Fig. 5C), we tested whether the mutant might preferentially grow toward hyperosmotic conditions in a split-agar assay used for measuring root hydrotropic responses among genotypes elongating at similar growth rates (*38*). Following transfer to split-agar plates with mannitol harboring asymmetric water availability, both WT and *aos* seedling roots readjusted their growth away from the hyperosmotic media in search for greater water availability (Fig. 6B and fig. S7, F and G). Contrary to our expectations, *kor1-4* roots also bent away from mannitol with a positive hydrotropic root curvature despite their slower growth rate. To our surprise, the JA-deficient *kor1-4 aos* double mutant failed to effectively readjust its root growth direction toward a greater water availability and instead grew into the mannitol media (Fig. 6C and fig. S7H). This effect was not a consequence of differential root thickness or the double mutant's inability to undergo general root bending responses such as those triggered by root gravitropism, but rather to a specific insensitivity to root hydrotropism (fig. S7, I to L). Consistently, while *esmd1-3* roots showed a normal root hydrotropic response, the *kor1-4 esmd1-3* double mutant with abolished constitutive root JA-Ile production was unable to redirect its root growth away from the mannitol media (fig. S7, M to P). Our data thus unveiled that the constitutive activation of JA-Ile production and signaling in *kor1-4* serves to facilitate root water foraging.

DISCUSSION

Plant cell walls are defining plant structures that serve a wide range of biological functions including shaping cell morphology, providing mechanical support for growth, and connecting cells within tissues. Changes in cell wall structure and assembly may have pronounced repercussions on intracellular and whole-plant responses (*21*). Here, we investigated how cues derived from perturbed cell walls integrate with the production of the stress hormone JA-Ile. The identification of cellulose-deficient *kor1* alleles displaying elevated JA-Ile levels specifically in seedling roots prompted us to examine cell wall–triggered induction of hormone biosynthesis in cell type–specific contexts. By restoring KOR1 function in specific layers of the primary root, we showed that ectopic JA-Ile signaling in endodermal and pericycle cells was caused by cell-nonautonomous signals deriving from adjacent and markedly enlarged cortex cells. Swollen *kor1* cortex cells could exert an increased mechanical pressure upon both external epidermal cells and inner tissues. As JA-Ile production is readily triggered by mechanical stress, why was the hormone increase observed only in inner tissues?

A possibility is that epidermal cells could dissipate the cortex-exerted mechanical pressure by expanding toward the available outer space and by stimulating cell division. Mechanical cues are known to influence cell cycle progression in animals, and although this has not yet been demonstrated in plants, they guide the orientation of plant cell division planes (*20*, *39*). Contrary to outer tissues, endodermal and pericycle cells are physically constrained and may become mechanically compressed by enlarged cortex cells. Reducing the swollen *kor1* cortex cell size in three independent manners fully abolished increased JA-Ile signaling in inner tissues. First, restoring KOR1 activity in the cortex complemented both cortex cell size and JA-Ile marker gene expression. Second, we identified a genetic suppressor of *kor1* that affected cell wall properties in which cortex cell size and JA-Ile levels were also restored. Third, by reducing *kor1* turgor pressure with hyperosmotic treatments, enlarged cortex cells and JA signaling were fully recovered. Our findings might explain why wounding single cells by laser ablation in living roots does not

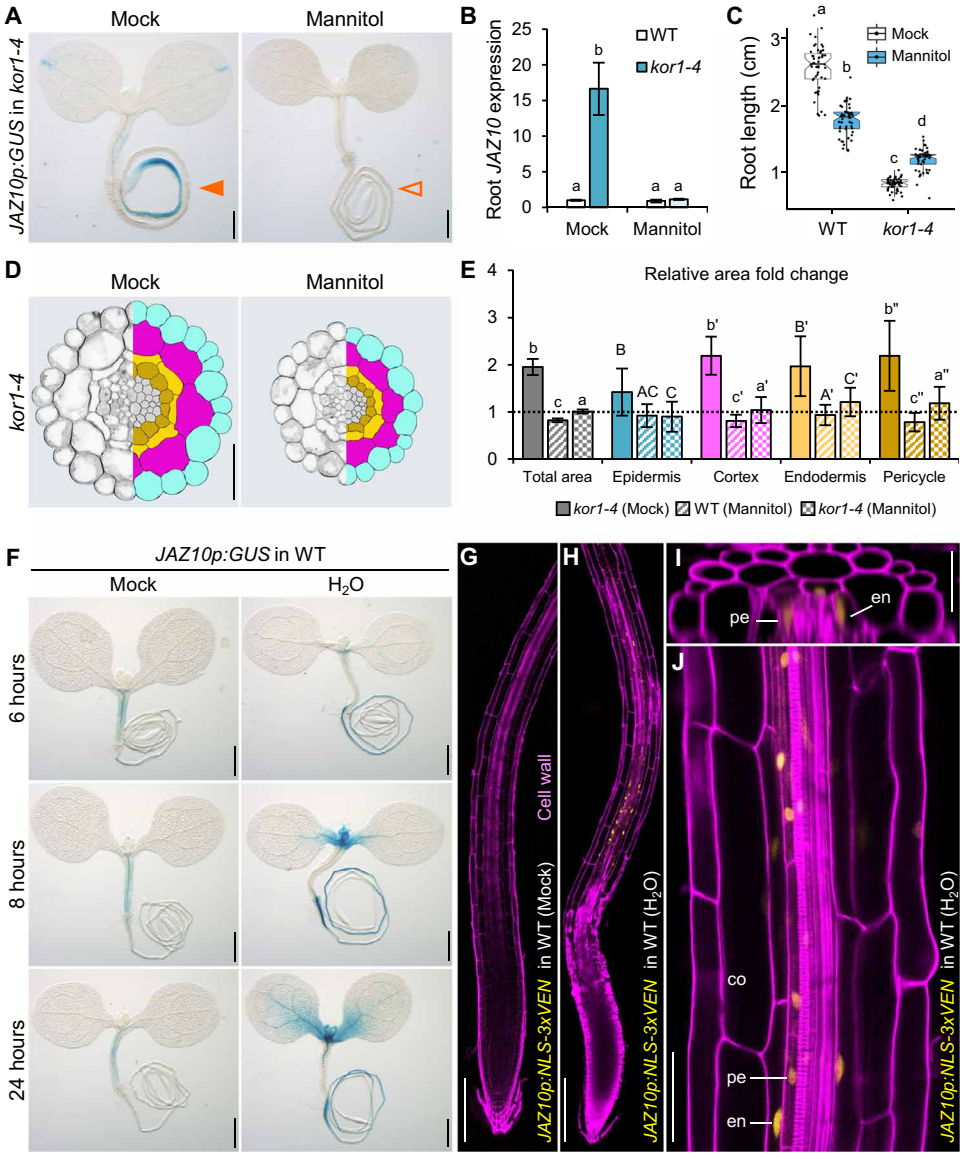

Fig. 5. Osmotic support abolishes constitutive JA production in *kor1*, while hypoosmotic treatment triggers JA-Ile signaling in WT. (**A**) Constitutive *JAZ10p:GUS* activity in *kor1-4* seedlings (orange arrowhead) is abolished following growth in 3% mannitol-supplemented media (empty arrowhead). (**B**) qRT-PCR of basal *JAZ10* root expression of indicated genotypes grown without (mock) or with mannitol. *JAZ10* levels were normalized to *UBC21*. Bars represent the means of three biological replicates (±SD), each containing pools of ~60 5-do roots. (**C**) Root length box plots of 7-do WT and *kor1-4* grown without or with mannitol. Medians are solid lines inside the boxes, and circles depict $n = 59$ to 61. Mannitol reduced WT root length by −0.78 cm, whereas it increased *kor1-4*'s by +0.35 cm (linear model, $P = 2 \times 10^{-6}$). (**D**) Representative split images from *kor1-4* root cross sections (left) and respective cell segmentations (right) grown without or with mannitol. (**E**) Total and cell-specific area fold change from segmented transversal root sections of WT and *kor1-4* grown without or with mannitol. Bars represent mean fold changes of individual cellular areas from 10 roots (±SD), normalized to mock-treated WT indicated by a dashed line (individual measurements are in fig. S6). (**F**) *JAZ10p:GUS* expression in WT seedlings submerged in isotonic solution (liquid MS, mock) or deionized water (H_2O) for the indicated time. (**G** to **J**) *JAZ10p:NLS-3xVEN* expression in WT roots submerged in (G) mock solution or (H) H_2O for 24 hours and counterstained with PI. (I) Orthogonal and (J) longitudinal view from the root early differentiation zone in (H). co, cortex; en, endodermis; pe, pericycle. Letters in (B), (C), and (E) denote statistically significant differences among samples as determined by ANOVA followed by Tukey's HSD test ($P < 0.05$). Scale bars, 0.5 mm (A and F), 50 μm (D and J), 200 μm (G and H), and 30 μm (I).

induce JA-Ile signaling (*27*). The disintegration of a target cell provokes adjacent cells to bulge toward the vacuity left by the ablated cell, in a process compatible from turgor pressure changes in adjacent cells due to the vanished support from the damaged cell (*40*, *41*). However, similarly to epidermal cells in *kor1*, wound-adjacent cells are not subjected to compression and might be able to compensate for the increased mechanical stress by expanding toward the void space without activating JA production. In addition to mechanical compression, a concomitant cause of JA-Ile production may reside in the mechanical tension generated between adjacent cells during cell elongation, possibly causing stretching imbalances in growing cells. In fact, JA-Ile signaling in *kor1-4* was observed immediately after the elongation zone and included sporadic activation in epidermal and cortical cells undergoing anisotropic extension. Collectively, the data

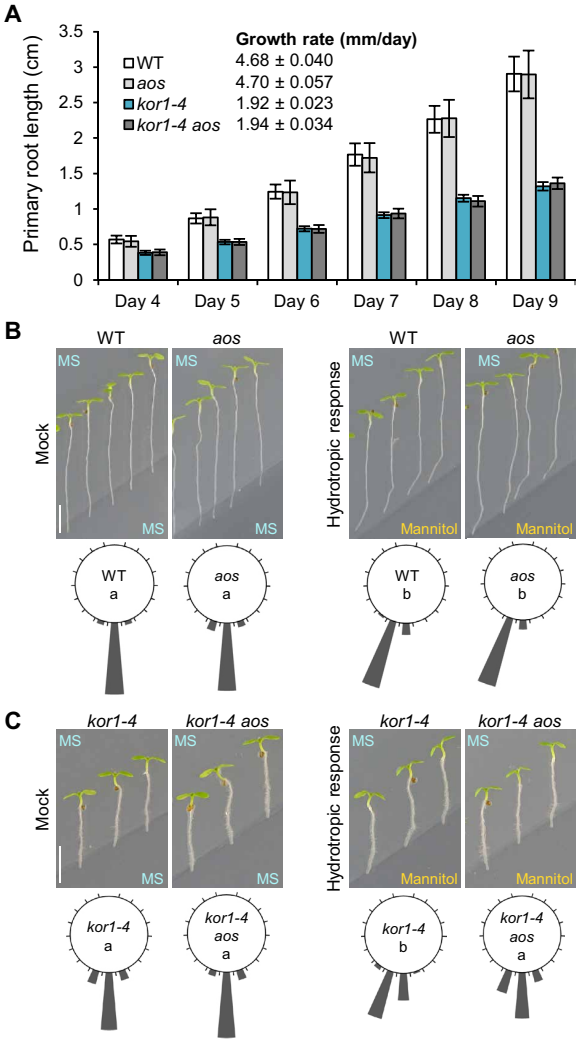

Fig. 6. Increased JA production facilitates *kor1* response to root hydrotropism. (**A**) Primary root elongation of indicated genotypes between 4 and 9 days after germination. Bars represent the means of 40 to 50 plants. Data were used to determine the root growth rate in millimeter per day by linear regression. (**B** and **C**) Root hydrotropic response of (B) WT and *aos* and (C) *kor1-4* and *kor1-4 aos* seedlings. Representative images and circular histograms summarizing root curvatures of indicated genotypes 24 hours after transfer to split-agar Murashige and Skoog (MS) plates under mock (MS/MS) or hydrotropism-inducing (MS/400 mM mannitol) conditions. Bars indicate the percentage of seedlings exhibiting a root bending angle assigned to one of the 1820° sectors on the circular diagram [individual measurements are available in fig. S7 (D and E)], $n = 42$. Letters indicate statistically significant differences as determined by two-way ANOVA followed by Tukey's HSD test ($P < 0.05$). Scale bars, 5 mm.

demonstrate that the JA pathway is triggered by turgor pressure–driven mechanical changes in response to cellulose deficiency.

Increases in turgor pressure by hypoosmotic treatment caused the induction of JA-Ile signaling also in inner tissues of WT roots, implying that turgor pressure–driven mechanical stress may be a general elicitor of JA-Ile production. Mechanical wounding and chewing insect herbivores squash tissues and possibly compress spatially constrained cells adjacent to wounds. Because cells within tissues are connected through their cell walls, mechanical stress signals arising from turgor pressure changes may propagate over distances depending on the extent of damage (*42*). Consistently, it has been proposed that mechanical tissue damage causes sudden pressure changes in vascular xylem vessels, leading to the compression of cells adjacent to vessels where JA biosynthesis is then initiated (*24*, *43*). Hence, turgor pressure changes generating mechanical compression may be a crucial elicitor of JA-Ile biosynthesis in circumstances extending beyond cell wall perturbations, with putative osmo- and mechanosensors located across different subcellular compartments (*44*). However, measuring mechanical stress patterns in vivo, particularly from cells embedded in inner tissues that are not physically accessible, remains challenging (*45*). Emerging tools are offering encouraging prospects to assess mechanobiological processes in vivo in future studies (*46*).

In our search to identify genetic regulators of ectopic JA-Ile production in *kor1* with potential roles in stress signals arising from turgor pressure changes, we did not retrieve known components involved in osmoregulation such as mechanically activated ion channels OSCA1 or MSL10, nor cell wall integrity sensors such as THESEUS1 whose loss of function was insensitive to isoxaben-induced JA production (*25*, *47*–*49*). This might be due to the screen not being saturated or to genetic redundancy. Instead, the *kor1* suppressor screen recovered an allele in *ESMD1*, a putative *O*-fucosyltransferase involved in pectin homeostasis (*31*). Although ESMD1's substrate and biochemical function are unknown, it was proposed that it may *O*-fucosylate cell wall integrity sensor proteins and thereby contribute to cell signaling (*31*). Recently, two enzymes belonging to the same GT106 family were shown to be rhamnosyltransferases involved in the biosynthesis of the pectin component rhamnogalacturonan I (RG-I) (*32*, *50*). Given that our monosaccharide composition analysis in genotypes with *esmd1-3* showed a substantial rhamnose reduction, which in *Arabidopsis* derives mostly from RG-I (*51*), and in agreement with other GT106 family members (*32*, *50*), ESMD1 may be directly involved in pectin biosynthesis. Although it remains unclear how *esmd1* restores cell shape and JA-Ile levels in *kor1*, RG-I can have significant and specific contacts with cellulose microfibrils (*52*). As turgor pressure is counterbalanced by cell walls being under tension (*53*), it is plausible that the diminished cell wall tensile strength in *kor1* is compensated by lack of *ESMD1*. The identification of ESMD1 also indicates that cell size and mechanical compression on inner tissues can be alleviated by remodeling cell wall properties and thus reequilibrate turgor pressure.

An unexpected observation was that constitutive JA-Ile signaling enabled *kor1* roots to modify their growth toward greater water availability. This finding highlights the importance of characterizing cell wall mutants as they may provide opportunities to uncover more subtle functions of the JA pathway. While the root hydrotropic response of the JA-deficient *aos* mutant did not differ from the WT, the suppression of constitutive JA-Ile production in *kor1-4 aos* and *kor1-4 esmd1-3* prevented roots to grow away from the media with reduced water availability. These findings imply that while JA deficiency per se does not affect root hydrotropism, ectopic JA-Ile signaling in precise tissues and cell types is beneficial for root water foraging. The heightened activation of JA signaling in *kor1* did not result in typical JA-mediated growth inhibition responses (*54*, *55*), suggesting that manipulating JA biosynthesis in specific cell types might confer acclimation advantages without hampering overall growth. As abscisic acid (ABA) perception in root cortical cells is required for WT root hydrotropic responses (*38*), ABA biosynthesis or signaling may be compromised in *kor1-4* cortex and counteracted

by constitutive JA-Ile production to redirect root growth. Hyperosmotic mannitol treatments are also used to study plant responses to water deficiency, and applying exogenous JA to various plants renders them more tolerant to drought, reviewed in (*56*). Accordingly, *Arabidopsis* mutants impaired in JA production or signaling are more drought-susceptible (*57*). Although it is unknown how constitutive JA signaling guides *kor1* roots away from mannitol, future studies deciphering the molecular mechanisms governing this effect could have beneficial impacts on breeding programs aimed at increasing plant drought tolerance.

MATERIALS AND METHODS

Plant material and growth conditions

A. thaliana accession Columbia (Col) was used for all experiments. *JAZ10p:GUSPlus* (*JGP*) transgenic lines in Col (WT) and in the JA-deficient *aos* mutant background were described previously (*6*). *JAZ10p:NLS3xVEN* was as in (*27*) but cloned and crossed into *aos* de novo. *kor1-6* (SALK_075812) and *esmd1-4* (GABI_216D03) were obtained from the Nottingham Arabidopsis Stock Centre (NASC), and *kor1-6* was crossed into *JGP* and *aos JGP*. *esmd1-1* was described in (*31*). For in vitro assays, seeds were sterilized and stratified 2 days at 4°C in the dark. Seedlings were grown on 0.5× solid Murashige and Skoog (MS; Duchefa) medium supplemented with MES hydrate (0.5 g/liter; Sigma-Aldrich) and 0.7 or 0.85% plant agar (AppliChem) for horizontal or vertical growth, respectively. Horizontally grown seedlings were germinated on a nylon mesh placed on top of the MS media as described (*6*). Controlled growth conditions were set at 21°C under light (100 µE m^{-2} s^{-1}), with a 14-hour light/10-hour dark photoperiod. For soil propagation, transformation, and crossing, plants were grown with the same temperature (*T*) and light intensity, but under continuous light.

Histochemical detection of GUS activity and lignin deposition

GUS stainings were performed as described (*58*) on a minimum of 20 individuals across experiments, and seedlings were photographed with a Leica M165 FC stereomicroscope fitted with a Leica MC170 HD camera. Lignin deposition was visualized by submerging seedlings in acidified phloroglucinol solution (1% phloroglucinol in 18% HCl) for 5 min, washing in 1× phosphate-buffered saline buffer, mounting in 10% glycerol, and imaging using differential interference contrast optics on a Leica DM6B microscope fitted with a Leica DMC6200 camera.

Plant treatments

Single cotyledon wounding of seedlings and MeJA (Sigma-Aldrich) treatments to assess *JGP* reporter activity were performed as described (*6*). To evaluate the JA response of the *JAZ10p:NLS-VEN* reporter in individual seedlings grown vertically, primary roots were mounted in mock or 10 µM MeJA 0.5× MS with PI (30 µg/ml; Sigma-Aldrich) solution, imaged immediately ($t = 0$) and after 2 hours ($n = 10$). For osmotic support experiments, plant growth media was supplemented with either 3% mannitol (165 mM; J&K Scientific), 3% sorbitol (165 mM; Carl Roth), 3% PEG 6000 (Serva), or 3% plant agar (AppliChem). For hypoosmotic treatments, seedlings were grown vertically for 5 or 7 days on MS media and then transferred to liquid isotonic solution (MS) or deionized water for the indicated times before GUS staining ($n = 20$) or confocal laser scanning microscopy (LSM) imaging ($n = 10$).

Gene expression analyses

RNA extraction and quantitative reverse transcription polymerase chain reaction (qRT-PCR) of *JAZ10* (At5g13220), *JOX3* (At3g55970), *VSP2* (At5g24770), and *UBC21* (At5g25760) were performed as described (*29*, *58*). Similarly, the expression of *JAZ3* (At3g17860) was assayed with GACTCGGAGCCACAAAAGC and TACGCTCGTGACCCTTTCTTTG and of *PDF1.2* (At5g44420) with TTTGCTGCTTTCGACGCAC and GCATGATCCATGTTTGGCTCC primers. RT-PCR of *KOR1* was performed with the primer pair AGATGCTGAAGCCAGAGCAG and TGTCATGGAGAGGTAATTCTGG.

JA-Ile quantification

5-do roots were excised beneath the collet region and flash-frozen to yield approximately 50-mg FW for each biological replicate. Extraction and quantitative measurements were performed as described (*29*). The limit of JA-Ile quantification (LOQ = 3× limit of detection) was determined from an *Arabidopsis* matrix as 0.49 pmol/g FW.

Cloning and generation of transgenic lines

All transcriptional and translational reporter constructs were generated by double or triple Multisite Gateway Technology (Thermo Fisher Scientific). ENTRY plasmids containing cell type–specific promoters (pEN-L4-*IRT1p*-L3, pEN-L4-*PEPp*-L3, pEN-L4-*SCRp*-L3, pEN-L4-*WOLp*-L3, and pEN-L4-*PIN1p*-L3) were described in (*30*) and obtained from NASC. pEN-L4-*JAZ10p*-R1, pEN-L1-*NLS-3xVEN*-L2, and pEN-R2-*CIT*-L3 were as in (*6*, *58*). CIT and mTurquoise (mT) fluorophores were subcloned into pDONR221 or pDONR-P2R-P3 to obtain pEN-L1-*CIT*-L2 and pEN-R2-*mT*-L3. Promoters were amplified from WT genomic DNA with oligonucleotides containing adequate restriction sites for *KOR1p* (GATGATGCTCTCTGATAAAGC and AAGTCTTTTGGGAGCTGCAA; 2.132 kb) and *ESMD1p* (ATCGACAGATCTCAATCTC and GGACGAGGACATCCTTGGTA; 2.168 kb) and cloned into pUC57 to create pEN-L4-*promoter*-R1 clones, as described (*58*). Coding DNA sequences of *KOR1* (ATGTACGGAAGAGATCCATG and TCAAGGTTTCCATGGTGCTG) and *ESMD1* (ATGCTAGCGAAGAATCGG and GGTGGCAGGAGGTGGTCTC) were amplified from WT complementary DNA with oligonucleotides specified in parenthesis containing appropriate *att* sites and recombined with pDONR221 or pDONR-P2R-P3 to obtain pEN-L1-*KOR1*-L2, pEN-L1-*ESMD1*-L2, and pEN-R2-*KOR1*-L3. For transcriptional reporters, pEN-L4-*JAZ10p*-R1 and pEN-L4-*ESMD1*-R1 were recombined with pEN-L1-*NLS-3xVEN*-L2 into pEDO097, as described (*58*). pEN-L4-*KOR1p*-R1 was also recombined with pEN-L1-*KOR1*-L2 into pEDO097 for complementation analysis. For translational reporters, pEN-L4-*KOR1p*-R1 or cell type–specific promoters were recombined with pEN-L1-*CIT*-L2 and pEN-R2-*KOR1*-L3 into a modified pH7m34gw vector named pFR7m34gw, which harbors seed red fluorescent protein (RFP) expression (*OLE1p:RFP*) instead of Hg resistance for in planta selection, to generate *promoter:CIT-KOR1* constructs. Similarly, to obtain *ESMD1p:ESMD1-mT* and *ESMD1p:ESMD1-CIT*, we recombined pEN-L4-*ESMD1p*-R1, pEN-L1-*ESMD1*-L2, and pEN-R2-*mT*-L3 or pEN-R2-*CIT*-L3 into pFR7m34gw (in both cases, fluorescence signals were undetectable, although the constructs were functionally complementing the mutant phenotype). All constructs were verified by Sanger sequencing, and transgenic plants were generated by floral dip with *Agrobacterium tumefaciens* strain GV3101. Transformed seeds expressing RFP in T_1, T_2, and T_3 generations were selected by fluorescence microscopy, and segregation analysis was

performed in >12 independent T_2 lines. A minimum of two independent T_3 transgenic lines were used for each construct to perform experiments and verify reproducibility.

Confocal microscopy

Confocal LSM imaging was performed on Zeiss LSM 700 or LSM 880 instruments. For live imaging, 5-do vertically grown seedling roots were mounted in 0.5× MS with PI (30 μg/ml). As *kor1* roots are thick and recalcitrant to PI penetration, *kor1* genotypes were fixed in 4% paraformaldehyde, cleared with ClearSee, and stained with Direct Red 23 (Sigma-Aldrich) as described (*59*). Excitation/detection ranges were set as follows: VENUS (VEN) and CIT: 514/515 to 545 nm; mT: 458/460 to 510 nm; Direct Red 23: 514/580 to 615 nm; PI: 561/600 to 700 nm. All images shown within one experiment were taken with identical settings and by analyzing at least 10 individuals per line. Image processing was performed in Fiji. Z-stacks were displayed as texture-based volume renderings using the 3D Viewer plugin of Fiji.

Suppressor screen and mapping by next-generation sequencing

Approximately 5000 seeds (0.1 g) of *kor1-4 JGP* were mutagenized with EMS (Sigma-Aldrich) as described (*6*). Resulting M_1 plants were either harvested individually (n = 1243) or in pools of 12 (n = 230). Twenty M_2 seedlings were screened from individually harvested plants, and 480 M_2s were screened from each pool to enlarge both the screening breadth and depth. A total of 135,260 M_2 seedlings, from 4003 M_1 plants, were assayed for lack of *JGP* activity in 5-do *kor1-4* seedlings by live GUS staining as described (*6*). To increase the screen stringency and avoid the recovery of false positives, M_2 seedlings were shifted from 21° to 26°C 24 hours prior GUS staining as *kor1* mutants are known exacerbate their phenotypes at higher T (*15*). Putative M_2 suppressors were transferred to soil and crossed to JA-deficient (*aos*, *opr3*, and *jar1*) and JA-insensitive (*coi1*) mutants to avoid the recovery of expected genes, and backcrossed to *kor1-4 JGP* for segregation analysis, phenotype confirmation, and mapping population development. *esmd1-3* was identified as a *JGP* suppressor of *kor1-4* by pooling 120 individuals lacking *JGP* reporter activity from a BC_1F_2 population and sequencing the bulk segregants by whole-genome sequencing. Genomic DNA extraction was as in (*6*). Library preparation (Illumina Shotgun TruSeq DNA PCR-free) and Illumina paired-end (PE) sequencing on a HiSeq X platform with 150-base pairs per read was performed by Macrogen. The output of 15 Gb resulted in an average of 118 sequencing depth for each base across the genome. EMS-generated single-nucleotide polymorphisms (SNPs) were identified as described (*6*), with updated software tools. Sequence reads were mapped to the TAIR10 *A. thaliana* genome with bowtie2 aligner (v. 2.3.1, parameter end-to-end). Alignment files were converted to BAM with SAMtools (v 1.8), and SNP calling was performed with GATK tool (v.4.1.0.0). Common SNPs with the *kor1-4 JGP* parental line were filtered out with the intersectBed tool from BEDTools utilities (v.2.22.1). The SNPEff tool (v.2.0.4 RC1) was used to predict the effect of the SNPs in coding regions. SNP frequencies (the number of reads supporting a given SNP over the total number of reads covering the SNP location) were extracted using the Unix command awk and plotted with R. Candidate SNPs were identified in genomic regions with high SNP frequencies (0.5 to 1) linked to the causal SNP, which had the expected frequency of 1. Validation of the candidate SNP was done by allelism test and by complementation by transformation.

Cell wall composition analysis

Alcohol-insoluble residue (AIR) was extracted from shoots and roots of 12-do seedlings as previously described (*60*). Each biological replicate consisted of ~100 shoots (~150-mg FW) or ~300 roots (~80-mg FW). A slurry solution of AIR [water (1 mg/ml)] was prepared for each sample and homogenized using a ball mill followed by sonication. Matrix polysaccharide composition of 300 μg of AIR after 2 M trifluoroacetic acid hydrolysis was analyzed via high-performance anion-exchange chromatography with pulsed amperometric detection (HPAEC-PAD), similar to (*60*), but on a 940 Professional IC Vario ONE/ChS/PP/LPG instrument (Metrohm) equipped with Metrosep Carb2 250/4.0 analytical and guard columns. Each run consisted of neutral sugar separation (22 min; 2 mM sodium hydroxide and 3.4 mM sodium acetate isocratic gradient), followed by uronic acid separation (23 min; 100 mM sodium hydroxide and 170 mM sodium acetate), and reequilibration (14 min; starting eluents) steps.

Cellulose was quantified on the basis of the two-step sulfuric acid hydrolysis method described by (*61*), with some modifications. Aliquots of AIR (200 μg each) were first pretreated with concentrated sulfuric acid (to swell cellulose) or were directly used for Seaman hydrolysis (to measure noncrystalline glucose) using ribose as an internal standard. Hydrolyzed glucose was quantified using the HPAEC-PAD system described above but with a shorter run: 2 mM sodium hydroxide and 3.4 mM sodium acetate isocratic gradient (22 min), followed by a 3-min rinse with 80 mM sodium hydroxide and 136 mM sodium acetate and a 4-min reequilibration with starting eluent.

Sectioning, segmentation, and cell analysis

Roots from vertically grown 5-do seedlings were vacuum infiltrated and fixed in glutaraldehyde:formaldehyde:50 mM sodium phosphate buffer (pH 7.2) (2:5:43, v/v/v) for 1 hour, dehydrated through an EtOH series, and embedded in Technovit 7100 resin (Heraeus Kulzer) as described (*58*). Samples were sectioned on a Microm HM355S microtome with a carbide knife (Histoserve) into 5-μm sections and mounted in 10% glycerol, and cell walls were visualized under dark field of a Zeiss AxioImager microscope fitted with an AxioCam MRm camera. TIF (tag image file format) images were segmented with PlantSeg (*62*) using preset parameters of the prediction model "lightsheet_unet_bce_dice_ds1x," which empirically segmented our images most accurately. For display purposes only, dark-field images were inverted, and segmented images were recolored in Photoshop to visualize different cell types more easily.

Root growth and tropism assays

Primary root length was evaluated in 7-do seedlings as described (*6*), and root growth rate was determined by measuring primary root length in 4-do seedlings for 6 consecutive days. Root diameter was assessed in 7-do seedlings by imaging vertically grown seedlings on a Leica M165 FC stereomicroscope fitted with a Leica MC170 HD camera, measuring the root thickness in the early differentiation zone (marked by the appearance of root hairs). For RAM measurements, 5-do seedlings were mounted in chloral hydrate:glycerol:water (8:2:1) solution and observed with a Leica DM6B microscope fitted with a Leica DMC6200 camera. The number of cells in the meristematic zone was counted in the cortex cell file between the quiescent center and the first elongating cell, as described (*6*). Root gravitropism assays were performed on vertically grown 5-do seedlings by rotating the plates by 90° and evaluating

root bending angles 24 hours after the rotation on scanned images with Fiji. For root hydrotropism assays, 5-do seedlings were transferred to split-agar plates containing either mock (MS/MS) or 400 mM mannitol (MS/mannitol) by aligning root tips 3 mm from the split-media boundary (*63*). Root bending angles were evaluated 24 hours after transfer to split-agar plates by analyzing scanned images with Fiji as described (*63*).

Statistical analysis

Box plots, multiple comparisons [analysis of variance (ANOVA) followed by Tukey's honest significant difference test].

SUPPLEMENTARY MATERIALS

Supplementary material for this article is available at http://advances.sciencemag.org/cgi/content/full/7/7/eabf0356/DC1

View/request a protocol for this paper from *Bio-protocol*.

REFERENCES AND NOTES

1. G. A. Howe, I. T. Major, A. J. Koo, Modularity in jasmonate signaling for multistress resilience. *Annu. Rev. Plant Biol.* **69**, 387–415 (2018).
2. J. Browse, J. G. Wallis, *Arabidopsis* flowers unlocked the mechanism of jasmonate signaling. *Plants* **8**, 285 (2019).
3. Z. Yang, Y. Huang, J. Yang, S. Yao, K. Zhao, D. Wang, Q. Qin, Z. Bian, Y. Li, Y. Lan, T. Zhou, H. Wang, C. Liu, W. Wang, Y. Qi, Z. Xu, Y. Li, Jasmonate signaling enhances RNA silencing and antiviral defense in rice. *Cell Host Microbe* **28**, 89–103.e8 (2020).
4. A. A. Agrawal, Current trends in the evolutionary ecology of plant defence. *Funct. Ecol.* **25**, 420–432 (2011).
5. D. Goodspeed, E. W. Chehab, A. Min-Venditti, J. Braam, M. F. Covington, *Arabidopsis* synchronizes jasmonate-mediated defense with insect circadian behavior. *Proc. Natl. Acad. Sci. U.S.A.* **109**, 4674–4677 (2012).
6. I. F. Acosta, D. Gasperini, A. Chetelat, S. Stolz, L. Santuari, E. E. Farmer, Role of NINJA in root jasmonate signaling. *Proc. Natl. Acad. Sci. U.S.A.* **110**, 15473–15478 (2013).
7. I. A. Penninckx, B. P. Thomma, A. Buchala, J. P. Métraux, W. F. Broekaert, Concomitant activation of jasmonate and ethylene response pathways is required for induction of a plant defensin gene in Arabidopsis. *Plant Cell* **10**, 2103–2113 (1998).
8. Q. Guo, I. T. Major, G. A. Howe, Resolution of growth-defense conflict: Mechanistic insights from jasmonate signaling. *Curr. Opin. Plant Biol.* **44**, 72–81 (2018).
9. M. L. Campos, J.-H. Kang, G. A. Howe, Jasmonate-triggered plant immunity. *J. Chem. Ecol.* **40**, 657–675 (2014).
10. C. Wasternack, I. Feussner, The oxylipin pathways: Biochemistry and function. *Annu. Rev. Plant Biol.* **69**, 363–386 (2018).
11. S. Mielke, D. Gasperini, Interplay between plant cell walls and jasmonate production. *Plant Cell Physiol.* **60**, 2629–2637 (2019).
12. D. J. Cosgrove, Plant cell wall extensibility: Connecting plant cell growth with cell wall structure, mechanics, and the action of wall-modifying enzymes. *J. Exp. Bot.* **67**, 463–476 (2016).
13. L. Denness, J. F. McKenna, C. Segonzac, A. Wormit, P. Madhou, M. Bennett, J. Mansfield, C. Zipfel, T. Hamann, Cell wall damage-induced lignin biosynthesis is regulated by a reactive oxygen species- and jasmonic acid-dependent process in Arabidopsis. *Plant Physiol.* **156**, 1364–1374 (2011).
14. C. Ellis, I. Karafyllidis, C. Wasternack, J. G. Turner, The Arabidopsis mutant cev1 links cell wall signaling to jasmonate and ethylene responses. *Plant Cell* **14**, 1557–1566 (2002).
15. D. R. Lane, A. Wiedemeier, L. Peng, H. Höfte, S. Vernhettes, T. Desprez, C. H. Hocart, R. J. Birch, T. I. Baskin, J. E. Burn, T. Arioli, A. S. Betzner, R. E. Williamson, Temperature-sensitive alleles of *RSW2* link the KORRIGAN endo-1,4-β-glucanase to cellulose synthesis and cytokinesis in Arabidopsis. *Plant Physiol.* **126**, 278–288 (2001).
16. L. Lei, T. Zhang, R. Strasser, C. M. Lee, M. Gonneau, L. Mach, S. Vernhettes, S. H. Kim, D. J. Cosgrove, S. Li, Y. Gu, The jiaoyao1 mutant is an allele of korrigan1 that abolishes endoglucanase activity and affects the organization of both cellulose microfibrils and microtubules in arabidopsis. *Plant Cell* **26**, 2601–2616 (2014).
17. J. López-Cruz, I. Finiti, E. Fernández-Crespo, O. Crespo-Salvador, P. García-Agustín, C. González-Bosch, Absence of endo-1,4-β-glucanase KOR1 alters the jasmonate-dependent defence response to Pseudomonas syringae in Arabidopsis. *J. Plant Physiol.* **171**, 1524–1532 (2014).
18. L. Peng, Y. Kawagoe, P. Hogan, D. Delmer, Sitosterol-β-glucoside as primer for cellulose synthesis in plants. *Science* **295**, 147–150 (2002).
19. T. Vain, E. F. Crowell, H. Timpano, E. Biot, T. Desprez, N. Mansoori, L. M. Trindade, S. Pagant, S. Robert, H. Höfte, M. Gonneau, S. Vernhettes, The cellulase KORRIGAN is part of the cellulose synthase complex. *Plant Physiol.* **165**, 1521–1532 (2014).
20. O. Hamant, E. S. Haswell, Life behind the wall: Sensing mechanical cues in plants. *BMC Biol.* **15**, 59 (2017).
21. J. K. Polko, J. J. Kieber, The regulation of cellulose biosynthesis in plants. *Plant Cell* **31**, 282–296 (2019).
22. L. Peng, C. H. Hocart, J. W. Redmond, R. E. Williamson, Fractionation of carbohydrates in *Arabidopsis* root cell walls shows that three radial swelling loci are specifically involved in cellulose production. *Planta* **211**, 406–414 (2000).
23. A. Chaudhary, X. Chen, J. Gao, B. Lesniewska, R. Hammerl, C. Dawid, K. Schneitz, The Arabidopsis receptor kinase STRUBBELIG regulates the response to cellulose deficiency. *PLOS Genet.* **16**, e1008433 (2020).
24. E. E. Farmer, D. Gasperini, I. F. Acosta, The squeeze cell hypothesis for the activation of jasmonate synthesis in response to wounding. *New Phytol.* **204**, 282–288 (2014).
25. T. Engelsdorf, N. Gigli-Bisceglia, M. Veerabagu, J. F. McKenna, L. Vaahtera, F. Augstein, D. Van der Does, C. Zipfel, T. Hamann, The plant cell wall integrity maintenance and immune signaling systems cooperate to control stress responses in *Arabidopsis thaliana*. *Sci. Signal.* **11**, eaao3070 (2018).
26. S. Rips, N. Bentley, I. S. Jeong, J. L. Welch, A. von Schaewen, H. Koiwa, Multiple *N*-glycans cooperate in the subcellular targeting and functioning of *Arabidopsis* KORRIGAN1. *Plant Cell* **26**, 3792–3808 (2014).
27. P. Marhavý, A. Kurenda, S. Siddique, V. D. Tendon, F. Zhou, J. Holbein, M. S. Hasan, F. M. W. Grundler, E. E. Farmer, N. Geldner, Single-cell damage elicits regional, nematode-restricting ethylene responses in roots. *EMBO J.* **38**, e100972 (2019).
28. M. Li, F. Wang, S. Li, G. Yu, L. Wang, Q. Li, X. Zhu, Z. Li, L. Yuan, P. Liu, Importers drive leaf-to-leaf transmission of jasmonic acid in wound induced systemic immunity. *Mol. Plant* **13**, 1485–1498 (2020).
29. A. Schulze, M. Zimmer, S. Mielke, H. Stellmach, C. W. Melnyk, B. Hause, D. Gasperini, Wound-induced shoot-to-root relocation of JA-Ile precursors coordinates *Arabidopsis* growth. *Mol. Plant* **12**, 1383–1394 (2019).
30. M. M. Marquès-Bueno, A. K. Morao, A. Cayrel, M. P. Platre, M. Barberon, E. Caillieux, V. Colot, Y. Jaillais, F. Roudier, G. Vert, A versatile multisite gateway-compatible promoter and transgenic line collection for cell type-specific functional genomics in Arabidopsis. *Plant J.* **85**, 320–333 (2016).
31. S. Verger, S. Chabout, E. Gineau, G. Mouille, Cell adhesion in plants is under the control of putative O-fucosyltransferases. *Development* **143**, 2536–2540 (2016).
32. Y. Takenaka, K. Kato, M. Ogawa-Ohnishi, K. Tsuruhama, H. Kajiura, K. Yagyu, A. Takeda, Y. Takeda, T. Kunieda, I. Hara-Nishimura, T. Kuroha, K. Nishitani, Y. Matsubayashi, T. Ishimizu, Pectin RG-I rhamnosyltransferases represent a novel plant-specific glycosyltransferase family. *Nat. Plants* **4**, 669–676 (2018).
33. S. Bouton, E. Leboeuf, G. Mouille, M.-T. Leydecker, J. Talbotec, F. Granier, M. Lahaye, H. Höfte, H.-N. Truong, *QUASIMODO1* encodes a putative membrane-bound glycosyltransferase required for normal pectin synthesis and cell adhesion in Arabidopsis. *Plant Cell* **14**, 2577–2590 (2002).
34. J. Du, A. Kirui, S. Huang, L. Wang, W. J. Barnes, S. N. Kiemle, Y. Zheng, Y. Rui, M. Ruan, S. Qi, S. H. Kim, T. Wang, D. J. Cosgrove, C. T. Anderson, C. Xiao, Mutations in the pectin methyltransferase QUASIMODO2 influence cellulose biosynthesis and wall integrity in Arabidopsis thaliana. *Plant Cell* **32**, 3576–3597 (2020).
35. G. Mouille, M.-C. Ralet, C. Cavelier, C. Eland, D. Effroy, K. Hématy, L. M. Cartney, H. N. Truong, V. Gaudon, J.-F. Thibault, A. Marchant, H. Höfte, Homogalacturonan synthesis in Arabidopsis thaliana requires a Golgi-localized protein with a putative methyltransferase domain. *Plant J.* **50**, 605–614 (2007).
36. K. Hématy, P.-E. Sado, A. Van Tuinen, S. Rochange, T. Desnos, S. Balzergue, S. Pelletier, J.-P. Renou, H. Höfte, A receptor-like kinase mediates the response of *Arabidopsis* cells to the inhibition of cellulose synthesis. *Curr. Biol.* **17**, 922–931 (2007).
37. D.-L. Yang, J. Yao, C.-S. Mei, X.-H. Tong, L.-J. Zeng, Q. Li, L.-T. Xiao, T.-p. Sun, J. Li, X.-W. Deng, C. M. Lee, M. F. Thomashow, Y. Yang, Z. He, S. Y. He, Plant hormone jasmonate prioritizes defense over growth by interfering with gibberellin signaling cascade. *Proc. Natl. Acad. Sci. U.S.A.* **109**, E1192–E1200 (2012).
38. D. Dietrich, L. Pang, A. Kobayashi, J. A. Fozard, V. Boudolf, R. Bhosale, R. Antoni, T. Nguyen, S. Hiratsuka, N. Fujii, Y. Miyazawa, T.-W. Bae, D. M. Wells, M. R. Owen, L. R. Band, R. J. Dyson, O. E. Jensen, J. R. King, S. R. Tracy, C. J. Sturrock, S. J. Mooney, J. A. Roberts, R. P. Bhalerao, J. R. Dinneny, P. L. Rodriguez, A. Nagatani, Y. Hosokawa, T. I. Baskin, T. P. Pridmore, L. De Veylder, H. Takahashi, M. J. Bennett, Root hydrotropism is controlled via a cortex-specific growth mechanism. *Nat. Plants* **3**, 17057 (2017).
39. M. E. Fernández-Sánchez, S. Barbier, J. Whitehead, G. Béalle, A. Michel, H. Latorre-Ossa, C. Rey, L. Fouassier, A. Claperon, L. Brullé, E. Girard, N. Servant, T. Rio-Frio, H. Marie, S. Lesieur, C. Housset, J.-L. Gennisson, M. Tanter, C. Ménager, S. Fre, S. Robine, E. Farge, Mechanical induction of the tumorigenic β-catenin pathway by tumour growth pressure. *Nature* **523**, 92–95 (2015).
40. L. Hoermayer, J. C. Montesinos, P. Marhava, E. Benkova, S. Yoshida, J. Friml, Wounding-induced changes in cellular pressure and localized auxin signalling spatially coordinate restorative divisions in roots. *Proc. Natl. Acad. Sci. U.S.A.* **117**, 15322–15331 (2020).

41. W. Zhou, J. L. Lozano-Torres, I. Blilou, X. Zhang, Q. Zhai, G. Smant, C. Li, B. Scheres, A jasmonate signaling network activates root stem cells and promotes regeneration. *Cell* **177**, 942–956.e14 (2019).
42. A. Boudaoud, An introduction to the mechanics of morphogenesis for plant biologists. *Trends Plant Sci.* **15**, 353–360 (2010).
43. A. Kurenda, C. T. Nguyen, A. Chételat, S. Stolz, E. E. Farmer, Insect-damaged *Arabidopsis* moves like wounded *Mimosa pudica*. *Proc. Natl. Acad. Sci. U.S.A.* **116**, 26066–26071 (2019).
44. D. Basu, E. S. Haswell, Plant mechanosensitive ion channels: An ocean of possibilities. *Curr. Opin. Plant Biol.* **40**, 43–48 (2017).
45. A. J. Bidhendi, A. Geitmann, Methods to quantify primary plant cell wall mechanics. *J. Exp. Bot.* **70**, 3615–3648 (2019).
46. L. Michels, V. Gorelova, Y. Harnvanichvech, J. W. Borst, B. Albada, D. Weijers, J. Sprakel, Complete microviscosity maps of living plant cells and tissues with a toolbox of targeting mechanoprobes. *Proc. Natl. Acad. Sci. U.S.A.* **117**, 18110–18118 (2020).
47. D. Basu, E. S. Haswell, The mechanosensitive ion channel MSL10 potentiates responses to cell swelling in *Arabidopsis* seedlings. *Curr. Biol.* **30**, 2716–2728.e6 (2020).
48. S. E. Murthy, A. E. Dubin, T. Whitwam, S. Jojoa-Cruz, S. M. Cahalan, S. A. R. Mousavi, A. B. Ward, A. Patapoutian, OSCA/TMEM63 are an evolutionarily conserved family of mechanically activated ion channels. *eLife* **7**, e41844 (2018).
49. F. Yuan, H. Yang, Y. Xue, D. Kong, R. Ye, C. Li, J. Zhang, L. Theprungsirikul, T. Shrift, B. Krichilsky, D. M. Johnson, G. B. Swift, Y. He, J. N. Siedow, Z.-M. Pei, OSCA1 mediates osmotic-stress-evoked Ca^{2+} increases vital for osmosensing in *Arabidopsis*. *Nature* **514**, 367–371 (2014).
50. B. Wachananawat, T. Kuroha, Y. Takenaka, H. Kajiura, S. Naramoto, R. Yokoyama, K. Ishizaki, K. Nishitani, T. Ishimizu, Diversity of Pectin Rhamnogalacturonan I Rhamnosyltransferases in Glycosyltransferase Family 106. *Front. Plant Sci.* **11**, 997 (2020).
51. F. A. Pettolino, C. Walsh, G. B. Fincher, A. Bacic, Determining the polysaccharide composition of plant cell walls. *Nat. Protoc.* **7**, 1590–1607 (2012).
52. T. Wang, Y. B. Park, D. J. Cosgrove, M. Hong, Cellulose-pectin spatial contacts are inherent to never-dried arabidopsis primary cell walls: Evidence from solid-state nuclear magnetic resonance. *Plant Physiol.* **168**, 871–884 (2015).
53. S. Robinson, A. Burian, E. Couturier, B. Landrein, M. Louveaux, E. D. Neumann, A. Peaucelle, A. Weber, N. Nakayama, Mechanical control of morphogenesis at the shoot apex. *J. Exp. Bot.* **64**, 4729–4744 (2013).
54. M. L. Campos, Y. Yoshida, I. T. Major, D. de Oliveira Ferreira, S. M. Weraduwage, J. E. Froehlich, B. F. Johnson, D. M. Kramer, G. Jander, T. D. Sharkey, G. A. Howe, Rewiring of jasmonate and phytochrome B signalling uncouples plant growth-defense tradeoffs. *Nat. Commun.* **7**, 12570 (2016).
55. I. T. Major, Q. Guo, J. Zhai, G. Kapali, D. M. Kramer, G. A. Howe, A phytochrome B-independent pathway restricts growth at high levels of jasmonate defense. *Plant Physiol.* **183**, 733–749 (2020).
56. J. Ruan, Y. Zhou, M. Zhou, J. Yan, M. Khurshid, W. Weng, J. Cheng, K. Zhang, Jasmonic acid signaling pathway in plants. *Int. J. Mol. Sci.* **20**, 2479 (2019).
57. J.-M. Kim, T. K. To, A. Matsui, K. Tanoi, N. I. Kobayashi, F. Matsuda, Y. Habu, D. Ogawa, T. Sakamoto, S. Matsunaga, K. Bashir, S. Rasheed, M. Ando, H. Takeda, K. Kawaura, M. Kusano, A. Fukushima, T. A. Endo, T. Kuromori, J. Ishida, T. Morosawa, M. Tanaka, C. Torii, Y. Takebayashi, H. Sakakibara, Y. Ogihara, K. Saito, K. Shinozaki, A. Devoto, M. Seki, Acetate-mediated novel survival strategy against drought in plants. *Nat. Plants* **3**, 17097 (2017).
58. D. Gasperini, A. Chételat, I. F. Acosta, J. Goossens, L. Pauwels, A. Goossens, R. Dreos, E. Alfonso, E. E. Farmer, Multilayered organization of jasmonate signalling in the regulation of root growth. *PLOS Genet.* **11**, e1005300 (2015).
59. R. Ursache, T. G. Andersen, P. Marhavý, N. Geldner, A protocol for combining fluorescent proteins with histological stains for diverse cell wall components. *Plant J.* **93**, 399–412 (2018).
60. C. Voiniciuc, M. H.-W. Schmidt, A. Berger, B. Yang, B. Ebert, H. V. Scheller, H. M. North, B. Usadel, M. Günl, MUCILAGE-RELATED10 produces galactoglucomannan that maintains pectin and cellulose architecture in arabidopsis seed mucilage. *Plant Physiol.* **169**, 403–420 (2015).
61. T. H. Yeats, H. Sorek, D. E. Wemmer, C. R. Somerville, Cellulose deficiency is enhanced on hyper accumulation of sucrose by a H^+-coupled sucrose symporter. *Plant Physiol.* **171**, 110–124 (2016).
62. A. Wolny, L. Cerrone, A. Vijayan, R. Tofanelli, A. V. Barro, M. Louveaux, C. Wenzl, S. Strauss, D. Wilson-Sánchez, R. Lymbouridou, S. S. Steigleder, C. Pape, A. Bailoni, S. Duran-Nebreda, G. W. Bassel, J. U. Lohmann, M. Tsiantis, F. A. Hamprecht, K. Schneitz, A. Maizel, A. Kreshuk, Accurate and versatile 3D segmentation of plant tissues at cellular resolution. *eLife* **9**, e57613 (2020).
63. R. Antoni, D. Dietrich, M. J. Bennett, P. L. Rodriguez, Hydrotropism: Analysis of the root response to a moisture gradient. *Methods Mol. Biol.* **1398**, 3–9 (2016).

Acknowledgments: We thank E. E. Farmer for enabling the initiation of this work by gifting the *kor1-4* and *kor1-5* EMS alleles originally identified in his lab and for critical comments on the manuscript. We also thank G. Mouille for sharing *esmd1-1* seeds, I. F. Acosta for gifting the pFR7m34gw plasmid, C. Wagner for assistance with AIR sample preparation, B. Yang for HPAEC-PAD maintenance, C. Wasternack and members of the Gasperini lab for critical discussions. **Funding:** This work was supported by the Leibniz Institute of Plant Biochemistry from the Leibniz Association, the German Research Foundation (DFG grant GA2419/2-1) to D.G. and (DFG grant 414353267) to C.V., and a Marie Skłodowska-Curie postdoctoral fellowship to M.K.M. **Author contributions:** S.M. and D.G. designed research. S.M, M.Z., M.K.M., and D.G. performed research. S.M., M.K.M., R.D., and D.G. analyzed data. H.S. and B.H. quantified JA-Ile levels. C.V. performed cell wall composition analyses. S.M. and D.G. wrote the manuscript with input from all authors. **Competing interests:** The authors declare that they have no competing interests. **Data and materials availability:** All data needed to evaluate the conclusions in the paper are present in the paper and the Supplementary Materials. Additional data related to this paper may be requested from the authors.

Submitted 29 September 2020
Accepted 22 December 2020
Published 10 February 2021
10.1126/sciadv.abf0356

Citation: S. Mielke, M. Zimmer, M. K. Meena, R. Dreos, H. Stellmach, B. Hause, C. Voiniciuc, D. Gasperini, Jasmonate biosynthesis arising from altered cell walls is prompted by turgor-driven mechanical compression. *Sci. Adv.* **7**, eabf0356 (2021).